

# A three-dimensional imaging detector based on nano-scale silver-related defects in X- and gamma-ray-irradiated glasses

メタデータ	言語: eng 出版者: 公開日: 2017-10-03 キーワード (Ja): キーワード (En): 作成者: メールアドレス: 所属:
URL	<a href="http://hdl.handle.net/2297/44804">http://hdl.handle.net/2297/44804</a>

# **A three-dimensional imaging detector based on nano-scale silver-related defects in X- and gamma-ray-irradiated glasses**

Toshio Kurobori<sup>1\*</sup>, Yuka Yanagida<sup>2</sup>, and Yao Qiang Chen<sup>3</sup>

<sup>1</sup>*Graduate School of Natural Science and Technology, Kanazawa University, Kanazawa 920-1192, Japan*

<sup>2</sup>*Oarai Research Center, Chiyoda Technol Corporation, Oarai, Ibaraki 311-1313, Japan*

<sup>3</sup>*China Techwin Co., Ltd., Dongguan, Guangdong 523467, China*

E-mail: kurobori@staff.kanazawa-u.ac.jp

Ag-activated phosphate glass, which is the most commonly known radiophotoluminescent (RPL) material, has the capability to operate not only dosimeters but also two- and three-dimensional (2D and 3D) dose imaging detectors in the same host. This passive detector is based on radiation-induced, optically active nano-scale defects. In this work, the transient-state optical properties of the blue and orange RPL were investigated using a time-resolved spectrum technique for <sup>137</sup>Cs and <sup>60</sup>Co gamma-ray-irradiated Ag-activated phosphate glass. Specifically, the blue RPL intensity with a decay time of 5 ns as a function of the depth at the vicinity of the surface was systematically examined to clarify an accurate dose distribution within the glass. Moreover, a feasibility study into the use of an RPL Ag-activated phosphate glass detector for fluorescent nuclear track imaging was demonstrated using a confocal fluorescence image microscope for the first time.

## **1. Introduction**

Passive dosimeters based on the thermoluminescence (TL), optically stimulated luminescence (OSL), and radiophotoluminescence (RPL) phenomena have been widely used for personal, environmental and clinical dosimetry, where lithium fluoride doped with Mg, Cu, and P (LiF:Mg,Cu,P), carbon-doped aluminium oxide (Al<sub>2</sub>O<sub>3</sub>:C), and silver-activated phosphate glass (composed of Ag<sup>+</sup> and PO<sub>4</sub><sup>3-</sup>), respectively, have been the most commonly used materials.<sup>1)</sup> These materials also have the capability to operate not only common dosimeters but also two- and three-dimensional (2D and 3D) dose imaging detectors in the same host or in a host with only different impurities. In practice, reconstructed areal and volumetric dose images have been demonstrated and developed using Al<sub>2</sub>O<sub>3</sub>:C,Mg based on the RPL,<sup>2)</sup> silver-activated phosphate glass based on the

RPL,<sup>3,4)</sup> and LiF crystals and thin films based on photoluminescence (PL)<sup>5)</sup> as a tool for fluorescent nuclear track detectors (FNTDs),<sup>2,6)</sup> accurate X-ray dose imaging over large areas,<sup>4,7)</sup> nuclear track etch detectors,<sup>8)</sup> X-ray nano-imaging,<sup>5,9)</sup> and proton beam diagnostics.<sup>10)</sup> The aforementioned passive detectors are based on radiation-induced, optically active atomic-scale defects, or F-aggregate colour centres (CCs) within the materials, such as  $F_2^+(2Mg)$ -RPL centres in  $Al_2O_3:C,Mg$ ,  $Ag^0$  and  $Ag^{2+}$ -RPL CCs in Ag-activated phosphate glass and  $F_2$  and  $F_3^+$ -PL CCs in LiF; therefore, the intrinsic spatial resolution of these detectors will ultimately be several nanometres. Their principles of operation are very similar to each other, and these luminescent centres increase in proportion to radiation doses with a wide dynamic range, though the excitation and emission wavelengths are fairly different. Moreover, these types of luminescent detectors do not require wires, electronics or batteries during irradiation,<sup>2)</sup> which are prominent features of passive detectors, in comparison with active detectors such as a metal oxide semiconductor field effect transistor (MOSFET) and a flat panel detector, which has a spatial resolution of 100-150  $\mu m$ .<sup>1)</sup>

Recently, we demonstrated a novel disk-type 2D imaging detector with a diameter of 100 mm, which was rotated at a rate of 2400 rpm, utilising Ag-activated phosphate glass for the first time.<sup>3,4)</sup> Following this step, we also performed a comparative study of the 2D dose images acquired using a disk-type Ag-activated phosphate glass plate based on blue and orange RPL and those acquired using LiF thin films based on green and red PL.<sup>11)</sup>

In this paper, the steady- and transient-state optical properties of blue and orange RPL in X- and gamma-ray-irradiated Ag-activated phosphate glass are presented via a normal fluorescence spectrophotometer and a time-resolved spectral technique, respectively. Specifically, the time-resolved blue RPL intensity with a decay time of 5 ns as a function of

the depth at the vicinity of the surface is systematically examined. Moreover, a preliminary fluorescent nuclear track image from X-ray-induced luminescent defects in Ag-activated phosphate glass is demonstrated using a confocal fluorescence image microscope for the first time.

## **2. Experimental procedure**

### **2.1 Ag-activated phosphate glass**

A commercially available Ag-activated phosphate glass plate was used for the optical measurements and 2D and 3D imaging acquisitions. The weight composition of the material used in this study was the same as that of FD-7 (Asahi Techno Glass), i.e., 31.55% P, 51.16% O, 6.12% Al, 11.00% Na, and 0.17% Ag. For the above measurements, such as absorption, excitation, emission (RPL), time-resolved spectra and imaging, the samples were cut into rectangular plates of a suitable size (approximately  $10 \times 7 \times 1 \text{ mm}^3$ ) from a standard glass dosimeter plate ( $33 \times 7 \times 1 \text{ mm}^3$ ).

### **2.2 X- and gamma-ray irradiations**

X-ray irradiations were performed in air using an X-ray unit with a tungsten target operated at a voltage of 30-200 kV and a current of 10 mA. The energy dependence was determined by irradiations with narrow spectra X-ray beams. The specified mean energies were obtained by varying the operating potential and added filtration in the range 24-165 keV. The irradiations were performed at a distance of 1 m from the tube. The absorbed doses were delivered to the samples with a dose of 3.0 Gy.

Gamma irradiations were also performed at RT using  $^{137}\text{Cs}$  (662 keV) and  $^{60}\text{Co}$  (1.17,

1.33 MeV) sources that delivered doses of 500 mGy and 1.0 Gy. All the samples were heated to 100 °C for 10 min to suppress the ‘build-up’ kinetics after the X- and gamma-ray irradiations.<sup>12)</sup>

### 2.3 Steady- and transient-state optical properties of the samples

The optical absorption was determined at room temperature (RT) using a Hitachi U-3900H spectrophotometer with a 1 nm step. The RPL and excitation spectra were obtained using a Hitachi F-2500 fluorescence spectrophotometer with a 2.5 nm spectral bandwidth.

In contrast, the time-resolved spectra for the blue and orange RPL signals were acquired using the combination of a high-repetition-rate Q-switched laser (Spectra Physics, Explorer One) at 349 nm, a photonic multichannel analyser (Hamamatsu Photonics, PMA-12) and a delay/pulse generator (Stanford Research Systems, DG535), as illustrated in Fig. 1. The pulse duration of the laser was less than 5 ns full-width at half-maximum (FWHM) at a repetition rate of 1 kHz for a pulse energy of 120  $\mu\text{J}$  in this work. The area of the beam on the glass sample through a rectangular metal slit ( $3 \times 0.5 \text{ mm}^2$ ) and a cylindrical lens with a 60 mm focal length was  $3 \times 0.08 \text{ mm}^2$ , and the fluence was 71  $\mu\text{J}/\text{mm}^2$  (17  $\mu\text{J}/\text{pulse}$ ). The time-resolved RPL spectra were measured in the wavelength range from 300 to 700 nm with a 10 ns gate time using a PMA-12 analyser equipped with an image intensifier (II). The blue and orange RPL signals were acquired through a long-pass filter (Edmund Optics, 84-754) and an optical fibre with a 1-mm-diameter and a numerical aperture (NA) of 0.2. The transient-state dose distributions in the direction of the depth up to 0.4 mm within the Ag-activated phosphate glass were measured with a step of 5  $\mu\text{m}$ . In this work, all of the measurements for the steady-state and transient state spectra were corrected for the instrumental calibration.

## 2.4 3D image acquisition

For a fluorescent track image acquisition of X-ray irradiated Ag-activated phosphate glass, a confocal fluorescence image microscope (Nikon Instech, A1R+) was used. The sample was stimulated using 405 nm light from a laser diode. A 3D image with a  $79.58 \times 79.58 \mu\text{m}^2$  field of view and with a total of 109 images at depths between 0.885 to 95.58  $\mu\text{m}$  below the surface of the sample was reconstructed. A Nikon 0.75 NA objective lens (Plan APO  $\lambda$  20 $\times$ ) and scan zoom 8 $\times$  were used.

## 3. Results and discussion

The steady-state optical absorption, excitation, and emission (RPL) spectra in Ag-activated phosphate glass with a thickness of 1.0 mm after X-ray irradiation under an energy of 25 keV with a dose of 3 Gy are shown in Fig. 2(a). Typical excitation spectra consist of two different bands. One spectrum peaks at 310 nm for an emission at 560 nm attributed to the hole-trapped  $\text{Ag}^{2+}$  centres, and the other peaks at 270 and 340 nm for an emission at 460 nm attributed to the  $\text{Ag}_2^+$  (reaction:  $\text{Ag}^+ + \text{Ag}^0 \rightarrow \text{Ag}_2^+$ ) and electron-trapped  $\text{Ag}^0$  centres,<sup>13,14</sup> respectively.

Moreover, the corresponding RPL spectra excited by the commercially available laser lines, indicated by arrows, at 337 nm (a pulsed  $\text{N}_2$  laser), 349 nm (a Q-switched Nd:YLF laser), 375 nm (a cw laser diode) and 405 nm (a cw laser diode), as well as at a 310 nm peak of the excitation spectra for an X-ray irradiated sample, are also shown. In this work, the excitation wavelengths of 349 nm and 375 nm were used for acquiring the time-resolved spectra and reconstructed 2D and 3D images,<sup>11</sup> respectively. The RPL

intensity excited by a wavelength of 405 nm was much lower than that of other wavelengths. As described later, the 405 nm line was used in this work for acquiring the 3D fluorescent nuclear track images by a confocal fluorescence image microscope.

Figure 2(b) presents the RPL spectra of the Ag-activated phosphate glass under 340 nm excitation after  $^{60}\text{Co}$  and  $^{137}\text{Cs}$  gamma-ray irradiations with absorbed doses of 500 mGy and 1 Gy. The orange RPL intensity for gamma-ray irradiation was approximately 40 times lower than that of X-ray irradiation; moreover, the blue RPL intensity was higher in comparison with the orange RPL intensity in the case of gamma-ray irradiation, as shown in Fig. 2(b). Such a behaviour, i.e., the ratios of the orange to blue RPL intensity in Ag-activated phosphate glass, was strongly sensitive to the radiation types, such as alpha<sup>15)</sup> and gamma rays<sup>7)</sup>; to the pulse duration, such as a femtosecond laser;<sup>16)</sup> and to the irradiation conditions at different temperatures and excitation photon energy.<sup>17)</sup>

A set of the time-resolved RPL spectra over 80 curves at different depths, with a step of 5  $\mu\text{m}$  from -70 to 330  $\mu\text{m}$  within the sample, under  $^{60}\text{Co}$  and  $^{137}\text{Cs}$  gamma-ray irradiations and with a dose of 1 Gy, are shown in Figs. 3(a) and 3(b), respectively. Each RPL spectrum for a '0-delay' excited at 349 nm laser pulses was piled up, as shown in the figure. Here, '0-delay' represents the value of a delay for which the intensity of the luminescence emitted from a sample is a temporal maximum. The four broken lines indicate the peak wavelengths at 430 and 550 nm. Moreover, the peak wavelengths for the blue and orange RPL in the steady-state spectra, as respectively shown in Figs. 2(a) and 2(b), were markedly shifted from 460 (steady-state) to 430 nm (transient-state) for the blue RPL and from 560 (steady-state) to 550 nm (transient-state) for the orange RPL, with the different ratios of the orange to the blue RPL intensities.

As shown in Fig. 4, plotting the intensity of the bands that peaked at 430 and 550 nm versus the relative depth within the glass from -70 to 330  $\mu\text{m}$  revealed the dose distributions under  $^{60}\text{Co}$  and  $^{137}\text{Cs}$  gamma-ray irradiations with a dose of 1 Gy. The surface of the sample is shown at 0  $\mu\text{m}$  on the graph. Therefore, a 'minus-sign' presents the position in air. The blue and green RPL intensities from each layer at different depths were considered to correspond to the concentration of the radiation-induced  $\text{Ag}^0$  and  $\text{Ag}^{2+}$  CCs within the sample. The decay measurement indicated that the lifetime value of the 550 nm band consisted of fast and slow components, i.e., the values were compatible with the blue (4.5 ns) and orange (2300 ns) RPL.<sup>13)</sup> Moreover, it is found that the radiation-induced defect distributions formed within the glass under gamma-ray irradiations were approximately from the surface to (250 - 300)  $\mu\text{m}$  in depth. As a result, in the case of  $^{60}\text{Co}$  and  $^{137}\text{Cs}$  gamma-ray irradiations, almost all of the energies are deposited at small depths in the order of 300  $\mu\text{m}$ .

As the similar spectra of Fig. 3, a set of the time-resolved RPL spectra over 80 curves at different depths under X-ray irradiation were also measured, as shown in Fig. 5(a). The RPL spectra corresponding to the transient-state time scale were completely different from those corresponding to the steady-state time scale presented in Fig. 2(a). The reasons are as follows: the decay time of the blue RPL is much shorter than that of the orange RPL.<sup>13)</sup> The  $\text{Ag}^0$  and  $\text{Ag}^{2+}$  CCs emitting the blue and orange RPL in Ag-activated phosphate glass will never disappear unless the glasses are annealed at a high temperature of about 400  $^{\circ}\text{C}$ .<sup>15)</sup> Therefore, under the steady-state time scale the integrated orange RPL intensity with the long decay lifetime is enhanced in comparison with the integrated blue RPL intensity with the short decay lifetime. In addition, note that the peak wavelength for the

orange RPL spectrum was markedly shifted to a longer wavelength, from 560 (steady-state) to 650 nm (transient-state), upon UV-nanosecond-laser excitation.

Plots of the intensities of the bands that peaked at 450 and 650 nm versus the depth within the glass, as shown in Fig. 5(b), revealed the dose distributions. Unlike  $^{60}\text{Co}$  and  $^{137}\text{Cs}$  gamma-ray irradiated dose distributions, the X-ray irradiated dose distribution was much narrower than that of the gamma-ray irradiation. The formed dose distribution was approximately from the surface to a depth of 100  $\mu\text{m}$  within the sample. The X-ray tube was operated at 40 kV and 10 mA under an energy of 32 keV. The background noise of the blue and orange RPL measured for the non-irradiated sample was subtracted from each RPL signal of the irradiated sample.

Figure 5(c) shows a preliminary fluorescent track image of X-ray irradiated Ag-activated phosphate glass under an energy of 25 keV with a dose of 3 Gy taken with a confocal fluorescence image microscope. The bright tracks are considered to be fluorescence from X-ray induced luminescent  $\text{Ag}^{2+}$  CCs. The A1R+ microscope is normally used for applications in brain research, other neuroscience and *in vivo* imaging of living specimens; therefore, in this work, only a 405 nm line is available as the shortest wavelength for exciting Ag-activated phosphate glass. As shown in Fig. 2(a), it is found that the RPL signal from the sample was extremely weak for a 405 nm excitation. Such a reconstructed track image was originally developed using  $\text{Al}_2\text{O}_3:\text{C},\text{Mg}$  FNTDs<sup>2,18)</sup> by Landauer, Inc. as a novel tool of replacing CR-39 plastic nuclear track detectors (PNTDs).

However, to obtain an accurate 3D dose distribution within the sample, it should be necessary to calibrate or compare the measured depth distribution (i.e., concentration) of active luminescent centres produced by radiation irradiations, as shown in Figs. 4 and 5(b), with the deposited energy curves of the used X- and gamma-rays within the sample.

Recently, the proton irradiations of LiF bulk and thin films were simulated<sup>10)</sup> using the SRIM<sup>19)</sup> software package. If the SRIM and other software, including the PHITS<sup>20)</sup> based on the Monte Carlo particle transport simulation code, are available for our system, the energy loss is calculated as a function of the implantation depth in the Ag-activated phosphate glass for different types of radiation and energies.

The preliminary calculations were carried out. The projected range of a proton ion (normal incidence) in Ag-activated phosphate glass can be calculated by the SRIM 2013 code, which is approximately 23.9  $\mu\text{m}$  and is shown in Fig. 6. The figure represents the energy loss suffered by 1.45 MeV protons by ionisation creation as a function of the implantation depth inside the target, considering a mass density of 2.60  $\text{g}/\text{cm}^3$ . More than 99.8 % of the energy loss to electrons is by direct interaction with the ions, and the energy loss by the ions to phonons is almost zero. The results of the SRIM simulations for Ag-activated phosphate glass were similar to those obtained for the LiF crystal for protons of 1.45 MeV of energy, which is  $21 \pm 0.3 \mu\text{m}$ <sup>10)</sup>. The inset of Fig. 6 also shows the plot of the ion tracks for 100,000 ions into the target. Detailed simulations using the SRIM and PHITS and the corresponding measurements using protons and heavy charged particles (HCP) are now under consideration.

#### **4. Conclusions**

The data obtained in this study led to the following conclusions:

(1) The steady- and transient-state optical properties of the blue and orange RPL of gamma- and X-ray-irradiated Ag-activated phosphate glass were compared and discussed.

(2) The blue and orange RPL intensities as a function of the depth from the surface to 400  $\mu\text{m}$  were measured, and the dose distributions as a function of the implantation depth were measured for different types of radiation and energies.

(3) A fluorescent track image of X-ray-irradiated Ag-activated phosphate glass was taken with a confocal fluorescent image microscope, although a 405 nm laser line was not suitable for the excitation source.

(4) A comparative investigation between the experimental results of the time-resolved dose distributions and the 3D track images in this work and those of the corresponding SRIM and PHITS simulations will be useful to obtain the accurate behaviour within the target for the ion and photon irradiations.

(5) The use of the blue RPL with a short lifetime of 5 ns in Ag-activated phosphate glass should be suitable for real-time measurements of the radiative doses, as well as for simultaneous 2D and 3D imaging.

## **Acknowledgements**

We would like to thank Professor H. Nanto at the Kanazawa Institute of Technology for valuable discussions and Y. Koguchi, N. Takeuchi, Professor T. Yamamoto and the staff of Chiyoda Technol Corporation for their contributions to the insightful discussions and for their help with the irradiations. Furthermore, T.K. would like to thank T. Shirao at the Bio Science Sales Division of Nikon Instech Co., Ltd. for his technical imaging support, as well as H. Itoi at Kanazawa University for his help during measurements. This work was supported by JSPS, a Grant-in-Aid for Scientific Research (B), No. 26289362 and partially by JST A-step, AS262Z00986P.

## References

- 1) J. Seco, B. Clasie, and M. Partridge, *Phys. Med. Biol.* **59**, R303 (2014).
- 2) M. S. Akselrod and G. J. Sykora, *Radiat. Meas.* **46**, 1671 (2011).
- 3) T. Kurobori and S. Nakamura, *Radiat. Meas.* **47**, 1009 (2012).
- 4) T. Kurobori and A. Matoba, *Jpn. J. Appl. Phys.* **53**, 02BD14 (2014).
- 5) G. Baldacchini, F. Bonfigli, A. Faenov, F. Flora, R. M. Montoreali, A. Pace, T. Pikuz, and L. Reale, *J. Nanosci. Nanotechnol.* **3**, 483 (2003).
- 6) J.-M. Osinga, M. S. Akselrod, R. Herrmann, V. Hable, G. Dollinger, O. Jäkel, and S. Greilich, *Radiat. Meas.* **56**, 294 (2013).
- 7) T. Kurobori, H. Itoi, Y. Yanagida, and Y. Q. Chen, *Nucl. Instrum. Methods Phys. Res., Sect. A* **793**, 6 (2015).
- 8) S. Kodaira, Y. Miyamoto, Y. Koguchi, D. Maki, H. Shinomiya, K. Hanaoka, N. Hasebe, H. Kawashima, M. Kurano, H. Kitamura, Y. Uchihori, and K. Ogura, *Radiat. Meas.* **71**, 537 (2014).
- 9) S. Almagia, F. Bonfigli, I. Franzini, A. Lai, R. M. Montoreali, D. Pelliccia, A. Cedola, and S. Lagomarsino, *Appl. Phys. Lett.* **89**, 054102 (2006).
- 10) M. Piccinini, F. Ambrosini, A. Ampollini, M. Carpanese, L. Picardi, C. Ronsivalle, F. Bonfigli, S. Libera, M. A. Vincenti, and R. M. Montoreali, *J. Lumin.* **156**, 170 (2014).
- 11) T. Kurobori, Y. Miyamoto, Y. Maruyama, T. Yamamoto, and T. Sasaki, *Nucl. Instrum. Methods Phys. Res., Sect. B* **326**, 76 (2014).
- 12) A. L. Manninen, A. Koivula, and M. T. Nieminen, *Radiat. Prot. Dosim.* **151**, 1 (2012).
- 13) T. Kurobori, W. Zheng, Y. Miyamoto, H. Nanto, and T. Yamamoto, *Opt. Mater.* **32**, 1231 (2010).
- 14) J. A. Perry, *RPL Dosimetry, Radiophotoluminescence in Health Physics* (Adam Hilger, Bristol, U. K., 1987) p. 21.
- 15) Y. Miyamoto, H. Nanto, T. Kurobori, Y. Fujimoto, T. Yanagida, J. Ueda, S. Tanabe, and T. Yamamoto, *Radiat. Meas.* **71**, 529 (2014).
- 16) H. Nanto, Y. Miyamoto, T. Ohno, Y. Takei, T. Kurobori, and T. Yamamoto, *Procedia Eng.* **25**, 231 (2011).
- 17) W. Zheng, T. Kurobori, Y. Miyamoto, H. Nanto, and T. Yamamoto, *Radiat. Meas.* **46**, 1402 (2011).
- 18) G.M. Akselrod, M. S. Akselrod, E. R. Benton, and N. Yasuda, *Nucl. Instrum. Methods Phys. Res., Sect. B* **247**, 295 (2006).
- 19) J. F. Ziegler, M. D. Ziegler, and J. P. Biersack, *Nucl. Instrum. Methods Phys. Res., Sect. B* **268**, 1818 (2010).
- 20) <http://phits.jaea.go.jp/index.html>

## Figure Captions

**Fig. 1.** (Colour online) Acquisition setup for the measurement of the time-resolved RPL spectra of the X- and gamma-ray-irradiated Ag-activated phosphate glass (exaggerated size). A laser beam with a rectangular beam shape was incident on a side facet of the sample.

**Fig. 2.** (Colour online) Steady-state absorption, excitation and RPL spectra of Ag-activated phosphate glass after X-ray irradiation with a dose of 3 Gy. Excitation spectra were detected at 460 and 560 nm. RPL spectra were excited at corresponding available laser lines (i.e., 337, 349, 375, and 405 nm) and at a 310 nm peak (a). RPL spectra of Ag-activated phosphate glass after  $^{60}\text{Co}$  and  $^{137}\text{Cs}$  gamma-ray irradiations with doses of 1 Gy (solid line) and 500 mGy (dashed line) were excited at 340 nm (b).

**Fig. 3.** (Colour online) A set of time-resolved RPL spectra of Ag-activated phosphate glass after UV laser irradiation at 349 nm for a zero delay at different depths from -70 to 330  $\mu\text{m}$  within the sample under  $^{60}\text{Co}$  (a) and  $^{137}\text{Cs}$  (b) gamma-ray irradiations with a dose of 1 Gy. The dashed lines show the peak position of the blue (at 430 nm) and green (at 550 nm) bands.

**Fig. 4.** (Colour online) Plot of the time-resolved RPL intensity of the bands peaking at 430 and 550 nm vs. the depth from the surface under  $^{60}\text{Co}$  and  $^{137}\text{Cs}$  gamma-ray irradiated Ag-activated phosphate glass with a dose of 1 Gy.

**Fig. 5.** (Colour online) A set of time-resolved RPL spectra at different depths within the sample under X-ray irradiation at 40 kV and 10 mA (a). Plot of the time-resolved RPL intensity of the bands peaking at 450 and 650 nm vs. the depth from the surface in Ag-activated phosphate glass (b). A fluorescent nuclear track image after X-ray irradiation of Ag-activated phosphate glass with a dose of 3 Gy (c).

**Fig. 6.** (Colour online) Simulation of energy loss suffered by 1.45 MeV protons in Ag-activated phosphate glass as a function of the depth within the sample. The inset shows a picture of the collision cascades for 100,000 ions.

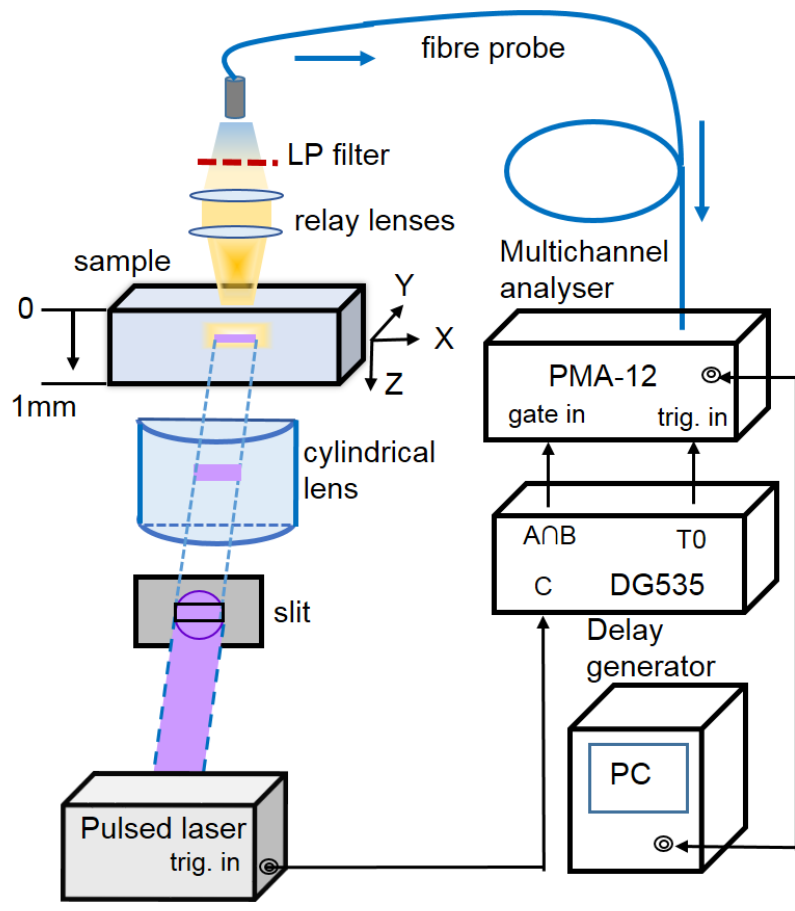


Fig. 1. (Colour Online)

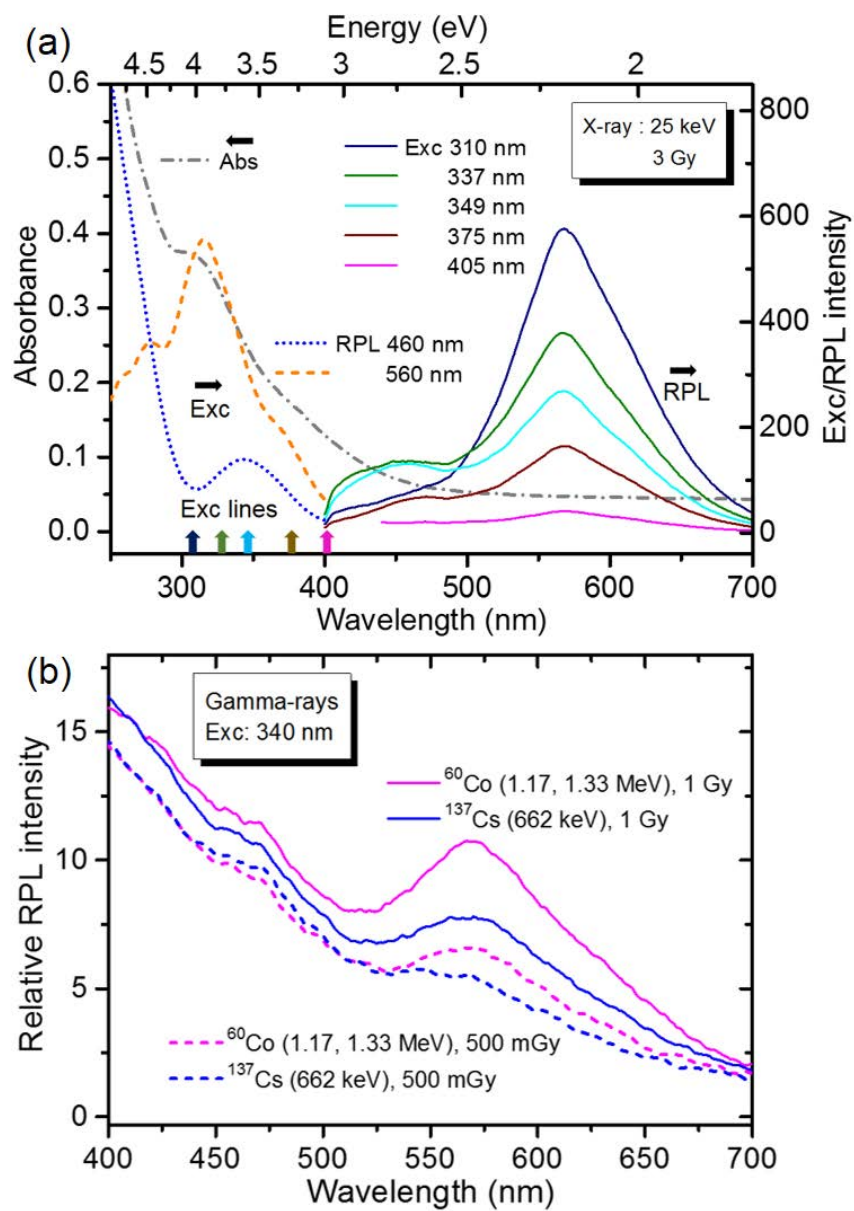


Fig. 2. (Colour Online)

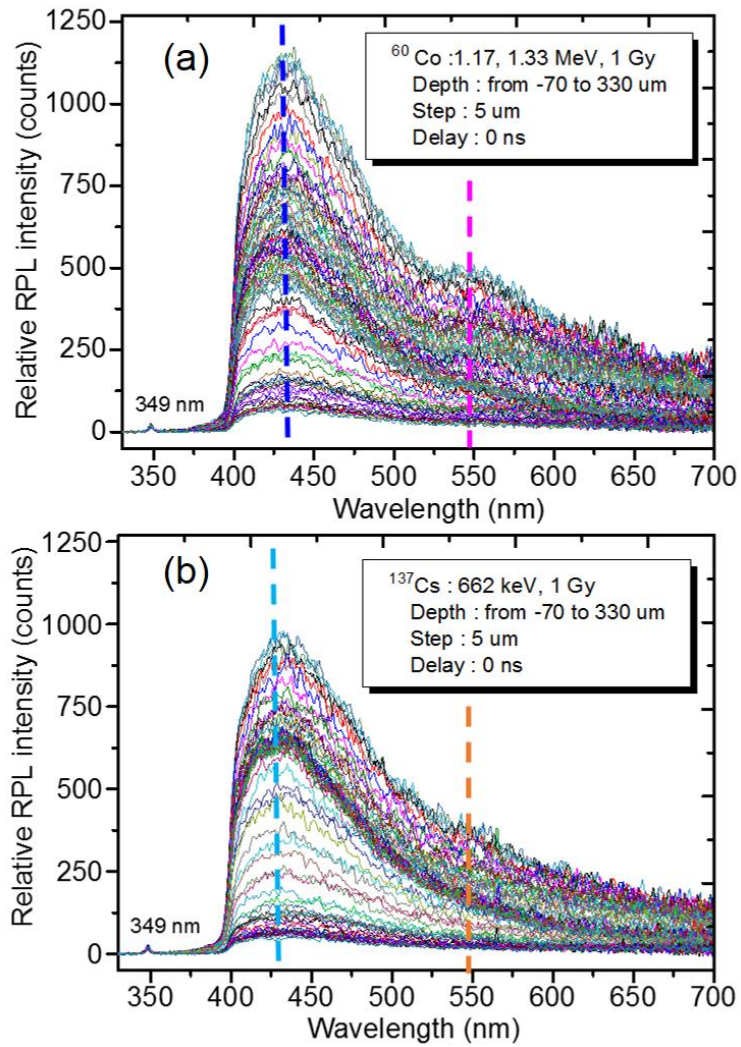


Fig. 3. (Colour Online)

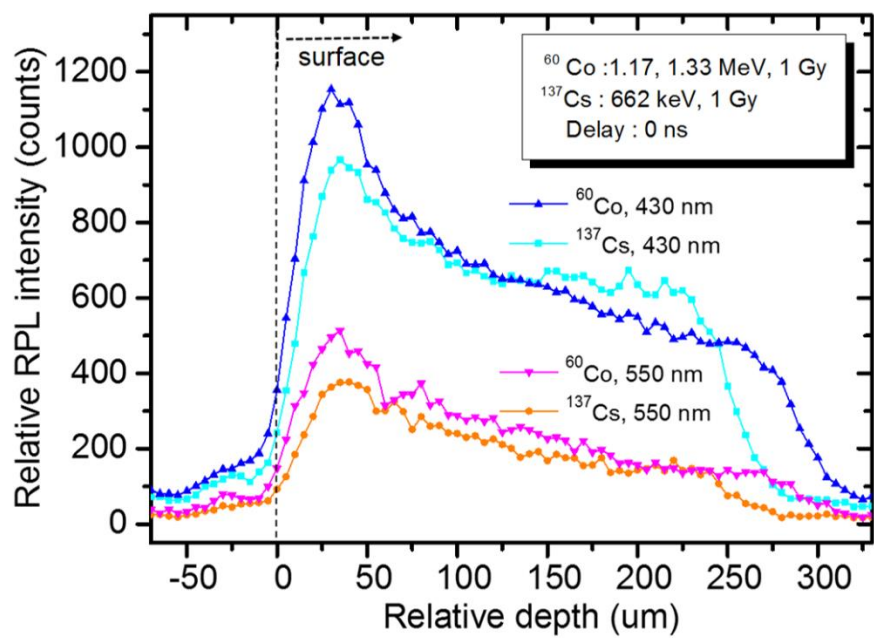


Fig. 4. (Colour Online)

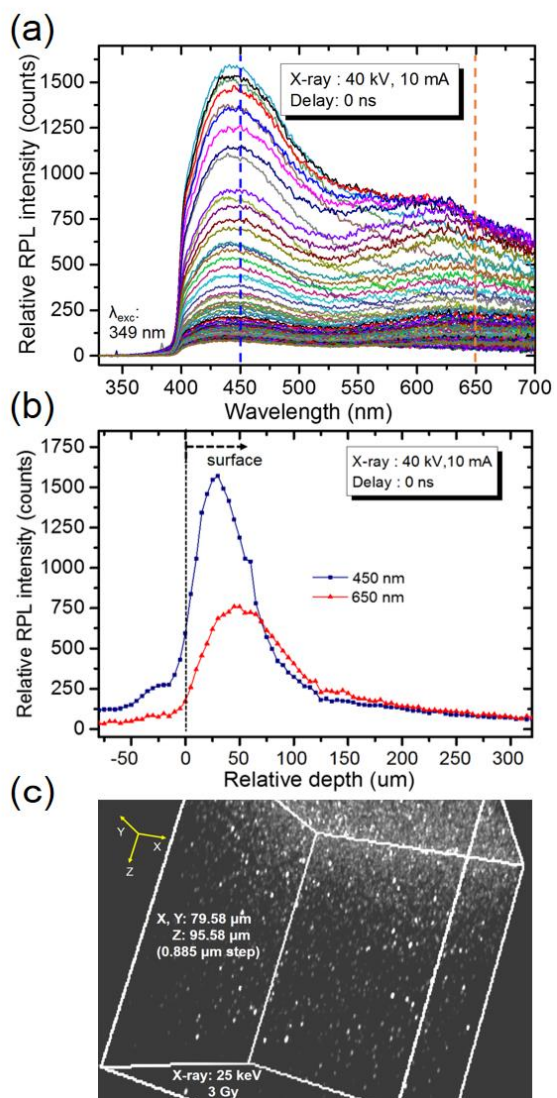


Fig. 5. (Colour Online)

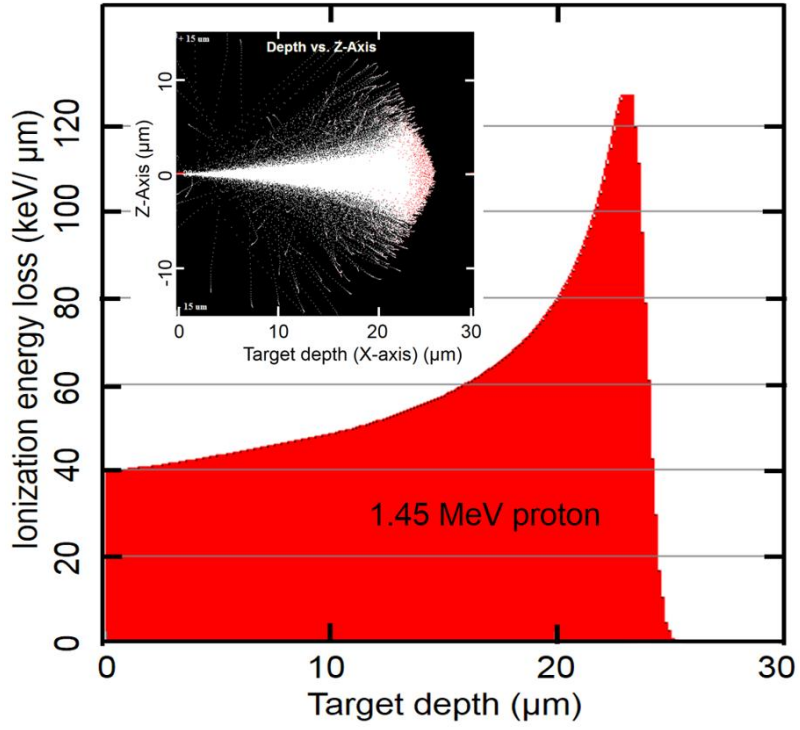


Fig. 6. (Colour Online)